Landslides (2023) 20:1719-1730 DOI 10.1007/s10346-023-02066-y Received: 5 May 2022 Accepted: 12 April 2023 Published online: 5 May 2023 © Springer-Verlag GmbH Germany, part of Springer Nature 2023

Shaojie Zhang 🗓 • Manyu Xia • Li Li • Hongjuan Yang • Dunlong Liu • **Fanggiang Wei** 



# Quantify the effect of antecedent effective precipitation on rainfall intensity-duration threshold of debris flow

Abstract  $\alpha$  and  $\beta$  are the two key parameters of the rainfall intensity-duration (ID) threshold curve for debris flow; the antecedent effective precipitation (AEP) poses influence on the ID threshold curve through changing  $\alpha$  and  $\beta$ . It is critical to explore the correlations of  $\alpha \sim AEP$  and  $\beta \sim AEP$  in order to quantify the influence of antecedent precipitation on ID threshold. However, the quantitative relationship between the AEP and the two parameters is still undetermined. In this study, a hydrological process-based numerical model that can derive the ID threshold curve is adopted to address this issue. Jiangjia Gully (JJG) in Dongchuan District of Yunnan Province, China, was chosen as the study area. The analysis results show that a higher AEP can provide favorable hydrological conditions for runoff generation and solid material resource recharge in JJG, but it do not always mean that the ID threshold condition for triggering debris flow is decreased. As for JJG, only after AEP > 40 mm, the AEP and ID threshold condition for triggering debris flow will be completely negatively correlated; when 15 mm≤AEP≤40 mm, the solid material supply is rapidly increased by the AEP, a stronger hydrodynamic condition is required to transform them into debris flow meaning that the ID threshold condition for triggering debris flow is enhanced in JJG, and this positive correlation between them persists until the two ID threshold curves intersect in the I-D coordinate system. AEP will significantly change the position of the threshold curve in the I-D coordinate system, and the change law of the position of the ID threshold curve can be described by the functions of  $\alpha \sim AEP$  and  $\beta \sim AEP$ . Due to the two functions, the ID threshold curve can regularly move in the I-D coordinate system rather than a conventional threshold curve stay the same regardless of AEP variation; it is beneficial to improve the prediction capacity of the ID threshold.

Keywords Antecedent effective precipitation · ID threshold · Debris flow · Debris flow density

### Introduction

Precipitation affecting debris flow formation includes triggering rainfall and antecedent effective precipitation (AEP) (Chen et al. 2005, 2018; Oorthuis et al. 2021). Increased AEP has been shown to enhance rainfall-induced runoff in various environments (Tisdall 1951; Luk 1985; Le Bissonnais et al. 1995; Castillo et al. 2003; Jones et al. 2017). Additionally, AEP decreases the shear strength of the loose soil mass in a debris flow gully, enhancing the supply rate of the solid material required for debris flow formation (Lehmann and Or 2012; Ruette et al. 2014). The rate of runoff generation and supply of solid material will directly influence the difficulty of triggering debris flow for the next following rainfall process. It can be seen that AEP has an important effect on the rainfall threshold of debris flow. Consequently, quantifying the effects of AEP on the rainfall threshold is helpful to improve the prediction precision for debris flow (Chen et al. 2018; Zhao et al. 2019; Hirschberg et al. 2021).

A rainfall threshold is generally a fixed value of some rainfall parameter such as cumulative rainfall, hourly rainfall intensity, or AEP (Marra et al. 2017); alternatively, it can be a curve of two rainfall parameters (Peres and Cancelliere 2014), such as the rainfall intensity-rainfall duration threshold curve (Caine 1980) and rainfall intensity-antecedent rainfall curve (Long et al. 2020). The most investigated threshold is the intensity (I) versus duration (D) curve (Crosta and Frattini 2003; Cannon et al. 2008; Guzzetti et al. 2008; Berti et al. 2020), which has the form  $I = \alpha D^{\beta}$ , where I represents the average rainfall intensity, D represents the rainfall duration, and α and β are empirical parameters. Segoni et al. (2018) analyzed the rainfall thresholds of landslides and debris flows reported in 107 articles and found that the threshold model based on the ID threshold curve accounted for the highest proportion, approximately 48.6%. Empirical and process-based methods are commonly used to derive the ID threshold curves of debris flow (Segoni et al. 2018). The empirical model workflow is as follows: debris flow events and the associated rainfall in a target area are collected, and the I and Dvalues of each rainfall process that triggered a debris flow event are calculated. D and I are plotted on the x and y axes, respectively, and the ID threshold curve is fitted using these data. As for the processbased methods, a physical parameter (P) that can represent debris flow occurrence in a gully is first chosen. During a rainfall process, P changes because of hydrological processes such as rainfall infiltration and runoff. Then, a numerical model is built to calculate P by inputting different rainfall conditions, the  $[D_i, I_i]$  data for which the calculated value is equal to Pis collected during model calculations. These collected data are then used to fit the threshold curves (Long et al. 2020). Papa et al. (2013) proposed that the total area (S) of shallow landslides induced by rainfall in a gully plays an important role in debris flow formation. Therefore, the ratio of S to the catchment area is used as P. The TRIGRS model (Baum et al. 2002, 2008) and a rainfall scenario simulation are used to calculate P and search for the combination of all  $[D_i, I_i]$  at which the calculated  $P_i$ is equal to a preset value. The ID threshold curve corresponding to the preset P is fitted by using these collected data. Although shallow landslides induced by rainfall are very important for debris flow formation, the effect of hydrodynamic conditions provided by rainfall-induced runoff on debris flow formation cannot be ignored. Scholars have argued that a water-soil mixture in a gully can be

formed by coupling between the rainfall-induced solid material and runoff (Church and Jakob 2020). The debris flow density represents the fluid characteristics of the mixture and can be used to incorporate the two major factors (rainfall-induced loose solid material and rainfall-induced runoff) that affect debris flow formation into numerical simulation models (Long et al. 2020). A numerical model is developed to correlate rainfall parameters with the debris-flow density (Zhang et al. 2020), which was denoted as Dens-ID here; the ID threshold curve of debris flow then can be constructed in the physical framework. The ID curve fitted by Dens-ID reportedly has a shape similar to that of the statistics-based curve. The precision of debris flow prediction by Dens-ID in Jiangjia Gully (JJG) in Yunnan Province, China, is approximately 80.5%, which is 27.7% higher than that of the statistics-based ID curve (Zhang et al. 2020).

The influence of AEP can be intuitively shown as changes in the positions of the ID threshold curves in the I-D coordinate system.  $\alpha$  and  $\beta$  are the two key parameters of the ID threshold curve of debris flow; they can reflect the variability of geological and hydrological conditions (Berti et al. 2020) and also can determine the position of the ID curve in the I-D coordinate system. Consequently, exploring the correlation of  $\alpha \sim AEP$  and  $\beta \sim AEP$ is critical for quantifying the effect of AEP on the ID threshold; however, an equation that describes the quantitative evolution of each parameter (α or β) with AEP has not been derived. Some studies have used the relationship between daily rainfall and antecedent rainfall (Kim et al. 1991; Glade et al. 2000; Dahal and Hasegawa 2008; Giannecchini et al. 2012) or a combination of daily rainfall intensity and rainfall duration (Hasnawir and Kubota 2008; Khan et al. 2012; Zhao et al. 2019; Kim et al. 2021; Yang et al. 2020) to investigate the effects of AEP on the rainfall threshold. However, all of these studies lack a quantitative description of the effect of AEP on the rainfall threshold due to complex field conditions (Berti et al. 2020).

To quantify the effect of AEP on the ID threshold curve, JJG in Yunnan Province, China, was chosen as the study area, and the Dens-ID was used to build its ID threshold curve database. The mechanism by which AEP affects the ID threshold curve is thoroughly discussed using this database, and equations for the functions describing the relationships between AEP and the parameters  $\alpha$  and  $\beta$  were derived through data analysis.

#### **Methods**

## **Dens-ID**

Shallow landslides and bed erosion are the two main sources of debris flow material; both may be present in the same gully, but one type is always dominant (Gabet and Mudd 2006; Berti and Simoni 2005; Coe et al. 2008; Long et al. 2020). Debris flow gullies with shallow landslides as the source of solid materials are widely distributed in southwestern China (Zhang et al. 2020). Dens-ID focuses on landslide-dominated supply and is designed to derive the ID threshold curves of debris flow by calculating the debris flow density in rainfall scenario simulations. The key function of this model is to correlate debris flow density with rainfall parameters, as described by Zhang et al. (2020) and Long et al. (2020). Debris flows are complex mixtures of water, fragmented rock, and sediments of all sizes (Chmiel et al. 2020). Dens-ID

simplifies this complex non-uniform flow (Iverson et al. 1997) as a water-soil mixture. The runoff and solid material are taken as the two parameters contributing to debris flow formation. Using these two parameters as the inputs of Eq. 1, Dens-ID can calculate the density of the water-soil mixture.

$$\rho_{\text{mix}}(t) = \frac{\rho_w V_w(t) + \rho_s V_s(t)}{V_{\text{mix}}(t)}$$
(1)

where  $\rho_{\text{mix}}$  is the density of the water-soil mixture,  $\rho_w$  is the water density,  $\rho_s$  is the density of soil particles, and  $V_{\text{mix}}$  is the volume of the water-soil mixture, which is the sum of  $V_w$  and  $V_s$ .  $V_w$  and  $V_s$  are the key variables for correlating the debris flow density with the rainfall parameters, which can be derived by pixel-based hydrological simulation (Long et al. 2020).

Based on a digital elevation model (DEM) of a debris flow gully, Dens-ID uses the theory of runoff generation from excess precipitation to control the infiltration boundary in the topsoil (Zhang et al. 2014a). It then simulates the vertical water movement within the soil mass using the differential equation of Richards (1931). Governing equation of infiltration border:

$$-D(\theta)\frac{\partial\theta}{\partial z} + K(\theta) = I(t) \tag{2}$$

Richards' differential equation:

$$\frac{\partial \theta}{\partial t} = \frac{\partial}{\partial z} [D(\theta) \frac{\partial \theta}{\partial z}]] - \frac{\partial K(\theta)}{\partial \theta}$$
(3)

where  $\theta$  is the soil-water content;  $D(\theta) = K(\theta)/(d\theta/d\psi)$  is the soil-water diffusivity; z is the soil depth, which is positive downward along the soil depth, taking the topsoil as the origin;  $K(\theta)$  is the hydraulic conductivity; I(t) is the rainfall intensity; and  $\psi$  is the soil matric suction.

After the hydrological simulation, Dens-ID outputs the watersoil content  $\theta(i, t)$ , soil matric suction  $\psi(i, t)$ , and runoff depth  $d_w(i, t)$  for each pixel of the DEM. Dens-ID then calculates  $V_w(t)$  using the runoff depth  $d_w(i, t)$ , as shown in Eq. 4.

$$V_{w}(t) = \sum_{t=1}^{T} \sum_{i=1}^{n} S_{g} * d_{w}(i, t)$$
(4)

where n represents the total number of grid cells that can generate runoff at time t,  $S_g$  represents the area of each pixel, and  $V_w(t)$  represents the total volume of runoff in a gully at time t. Using  $\theta(i, t)$  and  $\psi(i, t)$  as inputs, Dens-ID adopts the infinite slope model (Zhang et al. 2014b, 2018, 2021; Liu et al. 2016) to calculate the unstable depth of each grid cell  $d_s(j,t)$ . It then calculates  $V_s(t)$  using  $d_s(j, t)$ , as shown in Eq. 5.

$$V_{s}(t) = \sum_{t=1}^{T} \sum_{j=1}^{m} S_{g} * ds(j, t)$$
 (5)

where m represents the number of grid cells that can provide solid material at time t, and  $V_s(t)$  is the total volume of solid material in the gully at time t.

The mixture density can be derived by substituting various rainfall parameters, including rainfall intensity (I) and rainfall duration (D), into the right side of Eq. 2. Then, Dens-ID can correlate the rainfall parameters with the debris flow density.

# **Derivation of ID threshold curve using Dens-ID**

In nature, debris flow with a density  $\rho_{\text{mix}}$  can be triggered by high-intensity or long-duration rainfall. Inputting rainfall scenarios with different combinations of  $[I_i, D_i]$  into Dens-ID makes it possible to simulate debris flow initiation by rainfall in nature. Using a given density value  $(\rho_{\text{mix}})$  during the calculation, Dens-ID collects all the  $[I_i, D_i]$  data that meet the conditions of the rainfall scenarios (Fig. 1). That is, when the selected  $[I_i, D_i]$  are used as input, the output of the model is equal to  $\rho_{mix}$ . The collected  $[I_i, I_i]$  $D_i$  values represent another data group, which is referred to as a rainfall parameter set. Each data point  $[I_i, D_i]$  corresponds to a

unique value of  $\rho_{\text{mix}}$  within the density set; thus, the correlation between the rainfall parameters and debris flow density can then be established by Dens-ID. An ID curve can then be fitted through the collected  $[I_i, D_i]$  data to show the relationship between I and D. Each fitted ID curve corresponds to a unique  $\rho_{mix}$  within the density set, which is also considered to be the iso-density line (Zhang et al. 2020). The ID curves corresponding to a density value  $\rho_{mix}$  are fitted as follows:

Step 1: A typical density value was assigned to  $\rho_{mix}$ ; it can be determined after analysis of observation debris flow data, and assign a value to the AEP to Dens-ID.

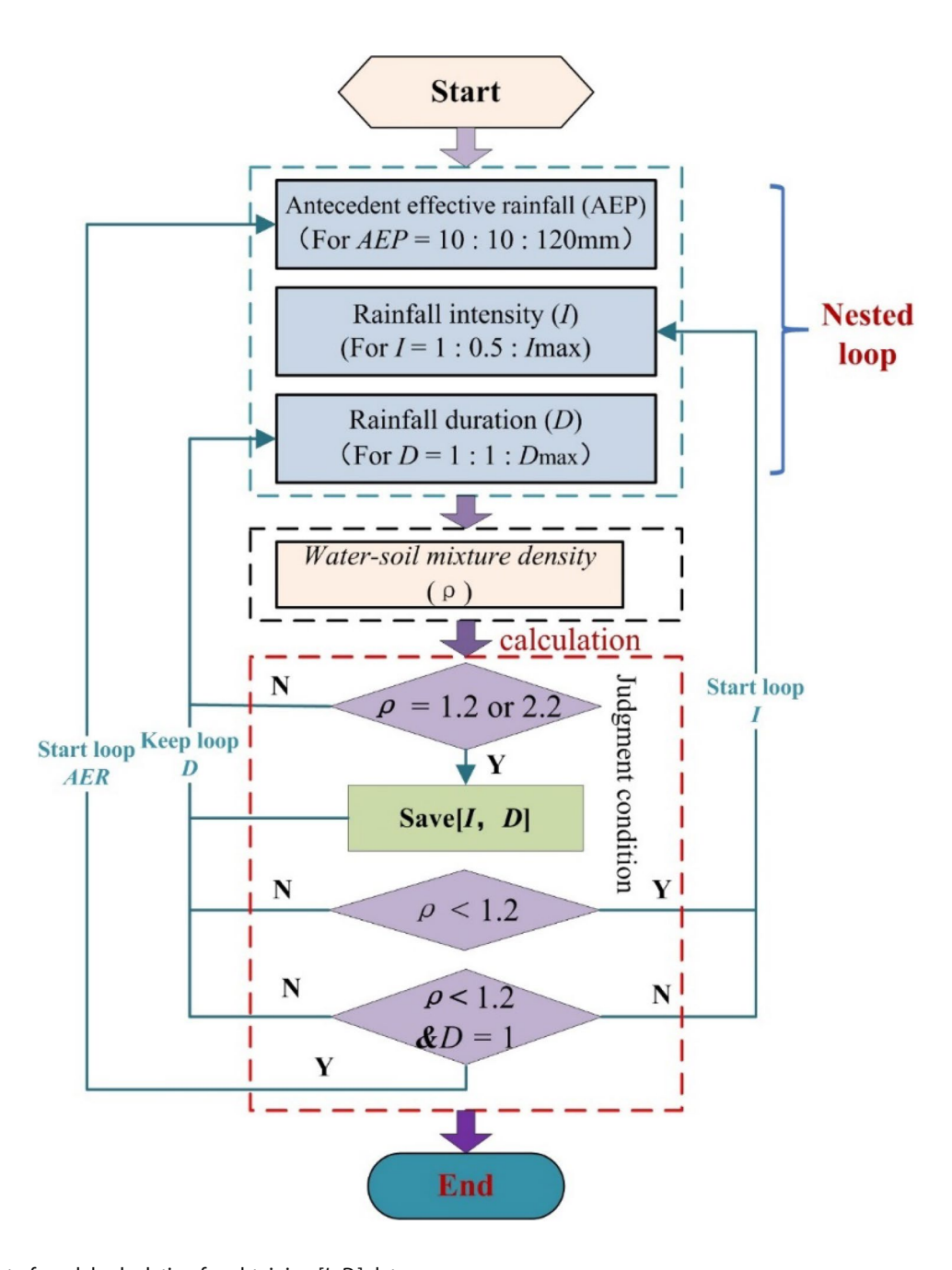


**Fig. 1** Flow chart of model calculation for obtaining  $[I_{ii}, D_{i}]$  data

Step 2: Assign a value to  $I_i$ , which generally represents the average rainfall intensity of a rainfall process that can trigger a debris flow and is held constant until the calculations in Step 4 are complete. The initial value of  $I_i$  is set to 1 mm/h. When Step 4 is complete,  $I_i$  is increased by 0.5 up to  $I_{D=1}$ . At  $I_{D=1}$ , a debris flow with density  $\rho_{\rm mix}$  can be triggered in the gully when D=1. Step 3: Under constant  $I_i$ , the calculation time of the model starts at t=1 h and increases by 1 h at each calculation step until  $t=D_i$ , where  $D_i$  represents the rainfall duration required to trigger a debris flow with density  $\rho_{\rm mix}$ . After  $t=D_i$ , the model calculation for a given  $I_i$  is complete.

Step 4: Repeat Steps 2 and 3 and collect the  $I_i$  and  $D_i$  values at which Dens-ID outputs the preset  $\rho_{\rm mix}$ . When the rainfall intensity  $I_i$  increases to  $I_{D=1}$ , the calculation for a given AEP<sub>i</sub> is complete. Thus, the data set of  $I_i$  and  $D_i$  for a certain AEP<sub>i</sub> is obtained, and the corresponding ID threshold curve can be fitted using these data.

Step 5: Repeat Steps 2, 3, and 4 and collect the  $I_i$  and  $D_i$  values. When AEP reaches the preset maximum value, the calculation for a given  $\rho_{mix}$  is complete.

#### Calculating the AEP using the observed rainfall data

The AEP was calculated as the weighted sum of rainfall periods before a debris flow (Long et al. 2020) and is expressed as follows:

$$AEP = \sum_{i=1}^{n} K^{n} R_{i}$$
 (6)

where the AEP is the antecedent effective rainfall; K is the attenuation coefficient, which is equal to 0.78 according to a field test in JJG (Cui et al. 2003); n is the number of days preceding the debris flow,  $R_i$  is the rainfall (mm) during day i.

# Study area and data collection

#### Jiangjia Gully

JJG is located in the Dongchuan district of Kunming City, Yunnan Province, China, and is the primary tributary of the Xiaojiang River. JJG has a drainage area of 48.6 km², and its elevation ranges from 1040 to 3260 m (Fig. 2). The terrain in JJG is steep; the relative relief between the ridge and valley is approximately 500 m, and most slopes have a gradient exceeding 25°. Menqian and Duozhao gullies, which are shown in Fig. 2, are the two main tributaries and account for 64.7% of the entire drainage area. Menqian Gully constitutes the initiation zones of debris flow in JJG (the initiation zone is surrounded by a lack curve in Fig. 2), and its channels are typically narrow and V-shaped (Fig. 3c). JJG is characterized by intense tectonism, and approximately 80% of the exposed rocks are highly fractured and slightly metamorphosed. Both rock types are weak and easily weathered and fragmented.

The slopes on both sides of JJG are covered by loose soil mass with tens of meters in thickness. Because of intense rainfall, shallow landslides frequently occur on the slopes and provide a large amount of loose solid material for debris flows (Fig. 3b). The steep terrain and large amount of loose solid material in JJG provide suitable conditions for debris flow formation. According to the collected rainfall data (Guo et al. 2013; Zhang et al. 2020),

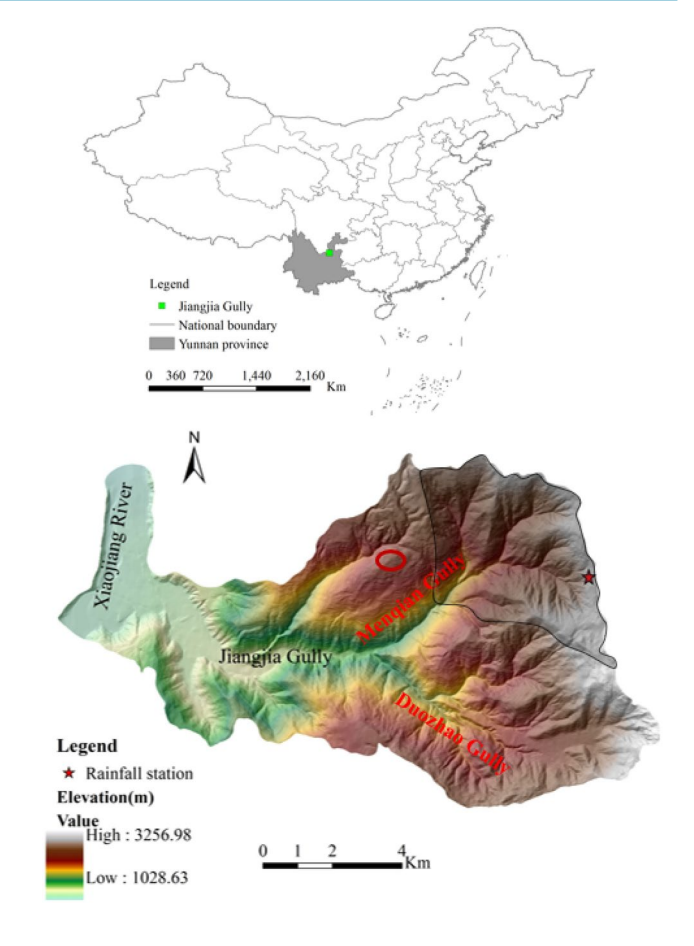


Fig. 2 Location of JJG

high-intensity or long-duration rainfall can trigger debris flow events. The solid material in JJG originates mainly from shallow landslides (Yang et al. 2022), which is consistent with the model

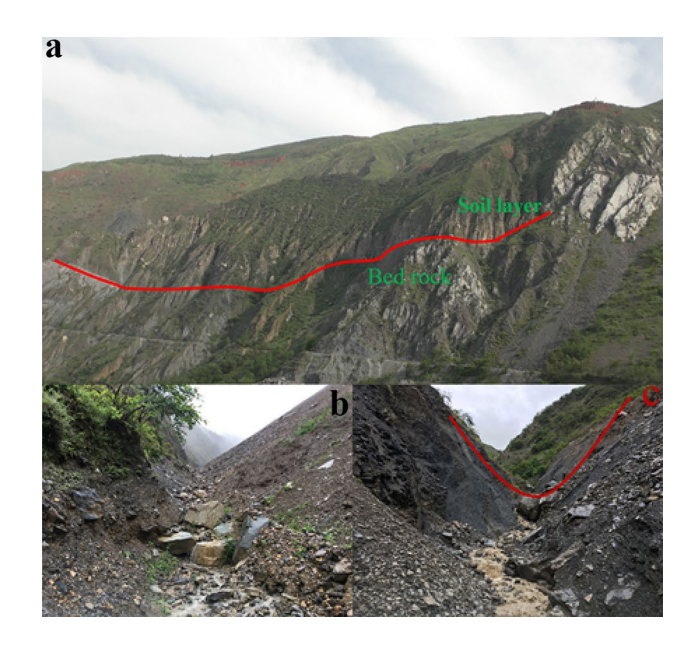


Fig. 3 Loose solid material in JJG

assumptions. Therefore, JJG is chosen as the study area to examine the effect of AEP on the ID threshold curves of debris flows.

#### Data for model calculation and validation

## ◆ Terrain data

DEM data for JJG were provided by the Dongchuan Debris Flow Observation and Research Station. The spatial resolution of the DEM is 0.5 m, and the data were obtained in December 2017 by aerial photogrammetry using an unmanned aerial vehicle. If the DEM with the accuracy of 0.5 m, 1 m, or 5 m was used as inputting, a large number of grids were generated and this situation can lead to memory overflow in Fortran programs. For computational efficiency reasons, aDEM with a grid size of 10 m was generated from the original terrain data using the resampling tools in ArcGIS. The DEM of JJG was used to derive the geometrical parameters of JJG such as slope length, gradient, and river channels.

## ◆ Data necessary for hydrological simulation

Three main soil types (Table 1) are distributed in IJG including dry red soil, red-yellow soil, and gravelly soil. Gravelly soil is widely distributed upstream in JJG and is the main source of solid material for debris flow. The hydrological parameters listed in Table 1 were obtained from the National Soil Database. In Table 1,  $\theta_c$  represents the saturated soil–water content,  $\theta_c$  is the residual water content,  $\alpha$  and n are the parameters of soil-water characteristic curve, which are used to calculate the matrix soil matric suction,  $f_c$  is the infiltration rate of the topsoil. The grid size of the land use map is 250 m, and its parameters, such as the normalized difference vegetation index, were obtained from the Moderate Resolution Imaging Spectroradiometer database. These data related to hydrological parameters were converted into a map with a grid size comparable to that of the DEM using the resampling tool in ArcGIS.

# ◆ Soil mechanical parameters

Soil cohesion c and internal friction angle  $\varphi$ , which are used in the infinite slope model, can be obtained through direct shear tests of soil samples from JJG. Most of the solid material for debris flows in JJG originates from gravelly soil; therefore, three groups of soil samples were taken from several typical slopes covered by a gravelly soil mass (the location of sampling was represented by red circle in Fig. 2), and one sample each was taken from the red-yellow and dry red soil. As shown in Table 2, the three samples from gravelly soils have similar c and  $\varphi$  values; therefore, the average values of the two parameters were calculated to represent the mechanical performance of the gravelly

**Table 1** Soil types and their hydrological parameters

Soil type	$\Theta_s$	$\Theta_r$	Parameters of curve		<i>f<sub>s</sub></i> (mm/h)
			α	n	
Gravelly soil	0.54017	0.07639	0.02201	1.37785	30.486
Red-yellow soil	0.48519	0.06829	0.02264	1.38146	21.964
Dry red soil	0.48148	0.07640	0.01476	1.47394	10.811

**Table 2** Cohesion c and internal friction angle  $\varphi$  of soil samples from JJG

Soil samples	Soil mechanical parameter				
	c (kPa)	φ (deg)	Average c (kPa)	Average φ (deg)	
Gravelly soil-1	35.1	36.0	34.5	34-4	
Gravelly soil-2	35.9	33.7	_		
Gravelly soil-3	32.5	33.7	_		
Red-yellow soil	27.0	36.3	27.0	36.3	
Dry red soil	25.9	35.7	25.9	35.7	

soil mass. The mechanical parameters in Table 2 can be assigned to each grid cell of the DEM according to the distribution of soil types in IIG.

## Historical debris flow and rainfall data

To validate the quantitative relationship between the AEP and the ID threshold curves of debris flows, data for 37 debris flow events in JJG and the triggering rainfall processes were collected. Rainfall events must be separated from long-term rainfall sequences to identify the rainfall processes that triggered the 37 debris flow events. The inter-event time (IET) was defined as a measure of the minimum time interval between two consecutive rainfall pulses (Adams et al. 1986). Although the IET strongly affects the start and end times of an event (Bel et al. 2017), there are no standard for rainfall episode separation (Jiang et al. 2021). Peres and Cancelliere (2018) noted that the IET depends on whether the rainfall during an IET is smaller than the mean daily potential evapotranspiration (MDPE). Long-term observation of the evaporation in JJG showed that the MDPE in this gully is approximately 4 mm; thus, precipitation of less than 0.5 mm during an IET is considered to indicate the end of a rainfall process (6).

## **Results and discussion**

# Historical data of debris flow events and rainfall

Using Eq. 6 and the collected rainfall data, the calculated AEP, average rainfall intensity (I), and rainfall duration (D) of each debris flow event can be determined and listed in Table 3. The calculated AEP values in the third column of Table 3 are rounded to integers to increase the number of debris flow events corresponding to each AEP. AEP values of 90 and 60 mm are associated with 1 debris flow event each, 8 events have an AEP value of 40 mm, 13 events have an AEP value of 30 mm, and 14 events have an AEP value of 20 mm. AEP calculated from the observation rainfall data varies from 11.5 mm to 92.6 mm. Referring to the range of AEP, Dens-ID presets several AEP values including 15, 20, 30, 40, 50, 60, 70, 80, 90, 100, 110, and 120 mm. The preset 110 and 120 mm exceeded the observed maximum value of 92.6 mm, because we wanted to observe whether the ID threshold curve would tend to stabilize after the AEP increased to a certain value.

**Table 3** Historical data of debris flow events and rainfall

34     1993/8/29     18.60     6.70     4.60     -       35     1998/8/2     18.40     3.70     7.30     -       36     2004/6/26     18.10     3.50     5.00     2.1	Number	Date	AEP (mm)	Rounded AEP (mm)	Duration (h)	Intensity (mm/h)	Density (g/cm³)
3       2008I/75       44.77       40       8.88       1.97       2.1         4       2001/74       42.50       21.7       1.40       2.0         5       2001/78       39.80       6.8       3.80       1.9         6       2008I/315       38.87       16.90       1.43       -         8       2007I/24       38.55       6.05       2.89       2.0         9       1999I/815       36.20       7.8       3.10       2.1         10       2006I/716       35.20       2.27       10.37       2.1         11       1999I/716       34.00       30       4       11.8       2.0         12       2008I/31       33.47       10.43       2.65       1.9         13       2000I/819       31.60       2.3       8.6       2.1         14       208.81/3       31.35       7.25       3.14       2.1         15       2010I/717       30.385       10.00       4.6       2.0         16       2020I/81/3       39.80       3.2       5.3       2.2         17       2079I/37       30.15       9.38       2.44       2.0         20	1	2004/7/9	92.60	90	9.30	1.00	1.8
4       2001/7/4       42.50       21.7       1.40       2.0         5       2001/7/8       39.80       6.8       3.80       1.9         6       2068/6/15       38.87       27.0       1.58       2.1         7       2008/6/15       38.87       16.90       1.43       -         8       2007/7/14       38.35       6.05       2.89       2.0         9       1999/8/15       36.20       2.8       3.10       2.1         10       2068/7/11       34.00       30       4       11.8       2.0         12       2068/7/21       33.47       10.43       2.65       1.9         13       2000/8/9       31.60       2.3       8.6       2.1         14       2008/8/3       31.35       7.25       3.14       2.1         15       2016/17       30.36       1.00       4.6       2.0         16       2001/17       30.35       1.00       4.6       2.0         17       2007/9/17       30.15       9.38       2.44       2.0         18       2016/18       29.80       3.2       5.3       2.2         2       20.08/17	2	2001/6/29	59.30	60	4.50	6.70	2.0
5       2001/7/8       39.80       6.8       3.80       1.9         6       2008/8/7       39.73       27.10       1.58       2.1         7       2008/6/15       38.87       16.90       1.43       -         8       2007/124       38.35       6.05       2.89       2.0         9       1999/8/155       36.20       2.7       10.37       2.1         10       2066/7/6       35.20       2.27       10.37       2.1         11       1999/7/16       34.00       30       4       11.8       2.0         12       2008/7/21       33.47       10.43       2.65       1.9         13       2000/8/9       31.60       2.3       8.6       2.1         14       2008/8/3       31.35       7.25       31.4       2.1         15       2010/7/17       30.385       1.00       4.6       2.0         16       2016/1/27       30.30       4       33.1       2.0         17       2007/9/17       30.15       9.38       2.44       2.0         18       2001/8/13       29.80       3.2       5.3       2.2         20       20.8/1/31<	3	2008/7/5	44.77	40	8.88	1.97	2.1
6       2008/8/7       39.73       27.10       1.58       2.1         7       2008/6/15       38.87       16.90       1.43       -         8       2007/7/24       38.35       6.05       2.89       2.0         9       1998/8/25       36.20       7.8       3.10       2.1         10       2006/7/6       35.20       2.27       10.37       2.1         11       1999/7/16       34.00       30       4       11.8       2.0         12       2008/7/21       33.47       10.43       2.65       1.9         13       2008/8/3       31.35       7.25       3.14       2.1         14       2008/8/3       31.35       7.25       3.14       2.1         15       2010/7/17       30.385       1.00       4.6       2.0         16       2016/6/27       30.30       4       13.1       2.0         17       2007/9/17       30.15       9.38       2.44       2.0         18       2018/13       29.80       3.2       5.3       2.2         20       2008/7/31       28.99       6.93       2.18       1.8         21       20.08/17	4	2001/7/4	42.50		21.7	1.40	2.0
7	5	2001/7/8	39.80	<u> </u>	6.8	3.80	1.9
8       2007/7/24       38.35       6.05       2.89       2.0         9       1999/8/25       36.20       7.8       3.10       2.1         10       2006/7/6       35.20       2.27       10.37       2.1         11       1999/7/16       34.00       30       4       11.8       2.0         12       2008/7/21       33.47       10.43       2.65       1.9         13       2000/8/9       31.60       2.3       8.6       2.1         14       2008/8/3       31.35       7.25       3.14       2.1         15       2010/7/17       30.385       1.00       4.6       2.0         16       20016/27       30.30       4       13.1       2.0         16       20016/17       30.30       4       13.1       2.0         17       2007/9/17       30.15       9.38       2.44       2.0         18       2001/8/13       29.80       3.2       5.3       2.2         20       2008/7/11       28.99       4.8       9.80       2.1         21       1994/6/26       29.00       3.50       6.00       2.2         23       2008/8/17 </td <td>6</td> <td>2008/8/7</td> <td>39.73</td> <td></td> <td>27.10</td> <td>1.58</td> <td>2.1</td>	6	2008/8/7	39.73		27.10	1.58	2.1
9 1999/8/25 36.20 7.8 3.10 2.1 10 2006/7/6 35.20 2.27 10.37 2.1 11 1999/7/16 34.00 30 4 11.8 2.0 12 2008/7/21 33.47 10.43 2.65 1.9 13 2000/8/9 31.60 2.3 8.6 2.1 14 2008/8/3 31.35 7.25 3.14 2.1 15 2010/7/7 30.385 1.00 4.6 2.0 16 2001/6/27 30.30 4 13.1 2.0 17 2007/9/17 30.15 9.38 2.44 2.0 18 2001/8/13 29.80 3.2 5.3 2.2 19 1994/6/26 29.00 2 2 23 - 20 2008/7/31 28.99 6.93 2.18 1.8 21 1999/7/24 28.90 4.8 9.80 2.1 22 2001/8/12 28.00 3.50 6.00 2.2 23 2008/8/17 26.29 3.75 3.23 1.8 24 2006/8/10 23.60 14.20 4.30 2.1 26 2006/8/8 23.50 5.00 14.20 4.30 2.1 26 2008/7/1 23.22 9.88 2.60 2.0 29 2010/7/6 22.376 10.88 4.18 2.1 30 2008/7/1 23.22 9.88 2.60 2.0 29 2010/7/6 22.376 10.88 4.18 2.1 31 2006/8/15 20.62 3.00 3.00 6.00 6.20 2.0 29 2010/7/6 22.376 10.88 4.18 2.1 31 2006/8/15 20.62 3.00 3.00 9.79 1.9 32 2006/7/15 19.60 6.00 6.20 2.0 35 1998/8/2 18.40 3.70 7.30 - 35 1998/8/2 18.40 3.70 7.30 - 36 2004/6/26 18.10 3.50 5.00 2.1	7	2008/6/15	38.87	<u> </u>	16.90	1.43	-
10	8	2007/7/24	38.35	<u> </u>	6.05	2.89	2.0
11	9	1999/8/25	36.20	<u>—</u>	7.8	3.10	2.1
12	10	2006/7/6	35.20		2.27	10.37	2.1
13	11	1999/7/16	34.00	30	4	11.8	2.0
14	12	2008/7/21	33.47	<u>—</u>	10.43	2.65	1.9
15	13	2000/8/9	31.60	<u>—</u>	2.3	8.6	2.1
16       2001/6/27       30.30       4       13,1       2.0         17       2007/9/17       30.15       9,38       2.44       2.0         18       2001/8/13       29.80       3.2       5.3       2.2         19       1994/6/26       29.00       2       23       -         20       2008/7/31       28.99       6.93       2.18       1.8         21       1999/7/24       28.90       4.8       9.80       2.1         22       2001/8/22       28.00       3.50       6.00       2.2         23       2008/8/17       26.29       3.75       3.23       1.8         24       2006/8/20       24.63       20       3.15       2.32       2.2         25       1999/8/10       23.60       14.20       4.30       2.1       2.2         26       2000/8/8       23.50       5.20       8.50       1.8         27       2008/7/1       23.22       6.00       6.20       2.0         28       2000/8/29       22.70       6.00       6.20       2.0         29       2010/7/6       22.376       3.66       4.8       4.18       2.1	14	2008/8/3	31.35	<u>—</u>	7.25	3.14	2.1
17	15	2010/7/17	30.385	<u>—</u>	1.00	4.6	2.0
18     2001/8/13     29.80     3.2     5.3     2.2       19     1994/6/26     29.00     2     23     -       20     2008/7/31     28.99     6.93     2.18     1.8       21     1999/7/24     28.90     4.8     9.80     2.1       22     2001/8/22     28.00     3.50     6.00     2.2       23     2008/8/17     26.29     3.75     3.23     1.8       24     2006/8/20     24.63     20     3.15     2.32     2.2       25     1999/8/10     23.60     14.20     4.30     2.1       26     2000/8/8     23.50     5.20     8.50     1.8       27     2008/7/1     23.22     9.88     2.60     2.0       28     2006/8/29     22.70     6.00     6.20     2.0       29     2010/7/6     22.376     10.88     4.18     2.1       30     2008/7/11     21.33     1.85     6.43     2.2       31     2006/8/15     20.62     3.08     9.79     1.9       32     2006/7/5     20.52     2.32     10.53     2.2       33     2006/7/15     19.60     3.70     7.30     -       34	16	2001/6/27	30.30		4	13.1	2.0
19	17	2007/9/17	30.15	<u> </u>	9.38	2.44	2.0
20	18	2001/8/13	29.80	<u> </u>	3.2	5.3	2.2
21       1999/7/24       28.90       4.8       9.80       2.1         22       2001/8/22       28.00       3.50       6.00       2.2         23       2008/8/17       26.29       3.75       3.23       1.8         24       2006/8/20       24.63       20       3.15       2.32       2.2         25       1999/8/10       23.60       14.20       4.30       2.1         26       2000/8/8       23.50       5.20       8.50       1.8         27       2008/7/1       23.22       9.88       2.60       2.0         28       2000/8/29       22.70       6.00       6.20       2.0         29       2010/7/6       22.376       10.88       4.18       2.1         30       2008/7/11       21.33       1.85       6.43       2.2         31       2006/8/15       20.62       3.08       9.79       1.9         32       2006/7/5       20.52       2.32       10.53       2.2         33       2000/7/15       19.60       26.2       2.90       1.7         34       1993/8/29       18.60       6.70       4.60       -         35	19	1994/6/26	29.00	<u> </u>	2	23	-
22     2001/8/22     28.00       23     2008/8/17     26.29       24     2006/8/20     24.63     20       25     1999/8/10     23.60     14.20     4.30     2.1       26     2000/8/8     23.50     5.20     8.50     1.8       27     2008/7/1     23.22     9.88     2.60     2.0       28     2000/8/29     22.70     6.00     6.20     2.0       29     2010/7/6     22.376     10.88     4.18     2.1       30     2008/7/11     21.33     1.85     6.43     2.2       31     2006/8/15     20.62     3.08     9.79     1.9       32     2006/7/5     20.52     2.32     10.53     2.2       33     2000/7/15     19.60     26.2     2.90     1.7       34     1993/8/2     18.60     6.70     4.60     -       35     1998/8/2     18.40     3.70     7.30     -       36     2004/6/26     18.10     3.50     5.00     2.1	20	2008/7/31	28.99	<u> </u>	6.93	2.18	1.8
23       2008/8/17       26.29       3.75       3.23       1.8         24       2006/8/20       24.63       20       3.15       2.32       2.2         25       1999/8/10       23.60       14.20       4.30       2.1         26       2000/8/8       23.50       5.20       8.50       1.8         27       2008/7/1       23.22       9.88       2.60       2.0         28       2000/8/29       22.70       6.00       6.20       2.0         29       2010/7/6       22.376       10.88       4.18       2.1         30       2008/7/11       21.33       1.85       6.43       2.2         31       2006/8/15       20.62       3.08       9.79       1.9         32       2006/7/5       20.52       2.32       10.53       2.2         33       2000/7/15       19.60       26.2       2.90       1.7         34       1993/8/29       18.60       6.70       4.60       -         35       1998/8/2       18.40       3.70       7.30       -         36       2004/6/26       18.10       3.50       5.00       2.1	21	1999/7/24	28.90	<u> </u>	4.8	9.80	2.1
24       2006/8/20       24.63       20       3.15       2.32       2.2         25       1999/8/10       23.60       14.20       4.30       2.1         26       2000/8/8       23.50       5.20       8.50       1.8         27       2008/7/1       23.22       9.88       2.60       2.0         28       2000/8/29       22.70       6.00       6.20       2.0         29       2010/7/6       22.376       10.88       4.18       2.1         30       2008/7/11       21.33       1.85       6.43       2.2         31       2006/8/15       20.62       3.08       9.79       1.9         32       2006/7/5       20.52       2.32       10.53       2.2         33       2000/7/15       19.60       26.2       2.90       1.7         34       1993/8/29       18.60       6.70       4.60       -         35       1998/8/2       18.40       3.70       7.30       -         36       2004/6/26       18.10       3.50       5.00       2.1	22	2001/8/22	28.00	<u> </u>	3.50	6.00	2.2
25       1999/8/10       23.60       14.20       4.30       2.1         26       2000/8/8       23.50       5.20       8.50       1.8         27       2008/7/1       23.22       9.88       2.60       2.0         28       2000/8/29       22.70       6.00       6.20       2.0         29       2010/7/6       22.376       10.88       4.18       2.1         30       2008/7/11       21.33       1.85       6.43       2.2         31       2006/8/15       20.62       3.08       9.79       1.9         32       2006/7/5       20.52       2.32       10.53       2.2         33       2000/7/15       19.60       26.2       2.90       1.7         34       1993/8/29       18.60       6.70       4.60       -         35       1998/8/2       18.40       3.70       7.30       -         36       2004/6/26       18.10       3.50       5.00       2.1	23	2008/8/17	26.29		3.75	3.23	1.8
26       2000/8/8       23.50       5.20       8.50       1.8         27       2008/7/1       23.22       9.88       2.60       2.0         28       2000/8/29       22.70       6.00       6.20       2.0         29       2010/7/6       22.376       10.88       4.18       2.1         30       2008/7/11       21.33       1.85       6.43       2.2         31       2006/8/15       20.62       3.08       9.79       1.9         32       2006/7/5       20.52       2.32       10.53       2.2         33       2000/7/15       19.60       26.2       2.90       1.7         34       1993/8/29       18.60       6.70       4.60       -         35       1998/8/2       18.40       3.70       7.30       -         36       2004/6/26       18.10       3.50       5.00       2.1	24	2006/8/20	24.63	20	3.15	2.32	2.2
27       2008/7/1       23.22       9.88       2.60       2.0         28       2000/8/29       22.70       6.00       6.20       2.0         29       2010/7/6       22.376       10.88       4.18       2.1         30       2008/7/11       21.33       1.85       6.43       2.2         31       2006/8/15       20.62       3.08       9.79       1.9         32       2006/7/5       20.52       2.32       10.53       2.2         33       2000/7/15       19.60       26.2       2.90       1.7         34       1993/8/29       18.60       6.70       4.60       -         35       1998/8/2       18.40       3.70       7.30       -         36       2004/6/26       18.10       3.50       5.00       2.1	25	1999/8/10	23.60		14.20	4.30	2.1
28       2000/8/29       22.70       6.00       6.20       2.0         29       2010/7/6       22.376       10.88       4.18       2.1         30       2008/7/11       21.33       1.85       6.43       2.2         31       2006/8/15       20.62       3.08       9.79       1.9         32       2006/7/5       20.52       2.32       10.53       2.2         33       2000/7/15       19.60       26.2       2.90       1.7         34       1993/8/29       18.60       6.70       4.60       -         35       1998/8/2       18.40       3.70       7.30       -         36       2004/6/26       18.10       3.50       5.00       2.1	26	2000/8/8	23.50		5.20	8.50	1.8
29       2010/7/6       22.376       10.88       4.18       2.1         30       2008/7/11       21.33       1.85       6.43       2.2         31       2006/8/15       20.62       3.08       9.79       1.9         32       2006/7/5       20.52       2.32       10.53       2.2         33       2000/7/15       19.60       26.2       2.90       1.7         34       1993/8/29       18.60       6.70       4.60       -         35       1998/8/2       18.40       3.70       7.30       -         36       2004/6/26       18.10       3.50       5.00       2.1	27	2008/7/1	23.22		9.88	2.60	2.0
30       2008/7/11       21.33       1.85       6.43       2.2         31       2006/8/15       20.62       3.08       9.79       1.9         32       2006/7/5       20.52       2.32       10.53       2.2         33       2000/7/15       19.60       26.2       2.90       1.7         34       1993/8/29       18.60       6.70       4.60       -         35       1998/8/2       18.40       3.70       7.30       -         36       2004/6/26       18.10       3.50       5.00       2.1	28	2000/8/29	22.70	<u> </u>	6.00	6.20	2.0
31     2006/8/15     20.62     3.08     9.79     1.9       32     2006/7/5     20.52     2.32     10.53     2.2       33     2000/7/15     19.60     26.2     2.90     1.7       34     1993/8/29     18.60     6.70     4.60     -       35     1998/8/2     18.40     3.70     7.30     -       36     2004/6/26     18.10     3.50     5.00     2.1	29	2010/7/6	22.376		10.88	4.18	2.1
32     2006/7/5     20.52     2.32     10.53     2.2       33     2000/7/15     19.60     26.2     2.90     1.7       34     1993/8/29     18.60     6.70     4.60     -       35     1998/8/2     18.40     3.70     7.30     -       36     2004/6/26     18.10     3.50     5.00     2.1	30	2008/7/11	21.33		1.85	6.43	2.2
33     2000/7/15     19.60     26.2     2.90     1.7       34     1993/8/29     18.60     6.70     4.60     -       35     1998/8/2     18.40     3.70     7.30     -       36     2004/6/26     18.10     3.50     5.00     2.1	31	2006/8/15	20.62		3.08	9.79	1.9
34     1993/8/29     18.60     6.70     4.60     -       35     1998/8/2     18.40     3.70     7.30     -       36     2004/6/26     18.10     3.50     5.00     2.1	32	2006/7/5	20.52		2.32	10.53	2.2
35 1998/8/2 18.40 3.70 7.30 - 36 2004/6/26 18.10 3.50 5.00 2.1	33	2000/7/15	19.60		26.2	2.90	1.7
36 2004/6/26 18.10 3.50 5.00 2.1	34	1993/8/29	18.60		6.70	4.60	-
	35	1998/8/2	18.40		3.70	7.30	-
37 2007/8/24 16.69 28.60 1.77 -	36	2004/6/26	18.10		3.50	5.00	2.1
	37	2007/8/24	16.69		28.60	1.77	-

In Table 3, the debris flow density in JJG varies from 1.6 to 2.2 g/ cm<sup>3</sup>, and its average is about 2.0 g/cm<sup>3</sup> with the mean square error of 0.15; debris flows with higher density are more easily triggered in JJG. Referring to this average value, Dens-ID assigned 2.0 g/cm<sup>3</sup> to  $\rho_{mix}$ , and then according to the "Derivation of ID threshold curve using Dens-ID" section, the ID threshold curve that corresponds to  $\rho_{mix}$  = 2.0 g/cm<sup>3</sup> will be derived and shown in the "ID threshold curves of debris flow with different AEP" section.

#### ID threshold curves of debris flow with different AEP

Based on Dens-ID, numerous calculations were performed following the steps in the "Derivation of ID threshold curve using Dens-ID" section and a database including all the data sets of [I, D], the fitted curves, and AEP was obtained and shown in Table 4.

All the fitted equation in Table 4 can be described by the power function; this result is consistent with the shape of the threshold curve obtained by the statistical model (Caine 1980), indicating that Dens-ID can describe the hydrological process of rainfall-induced debris flow. In order to show the influence of AEP more intuitively on the ID threshold curve, all the fitted equations in Table 4 excluding the curves corresponding to AEP = 100, 110, 120 mm are drawn in Fig. 4 with the logarithmic coordinate system.

We can find from Fig. 4 that the ID threshold conditions necessary for triggering debris flow in JJG do not always show a decreasing trend with the increasing AEP. There are two very significant inflection points here including AEP = 40 mm and AEP = 90 mm. As shown in Fig. 4a, the four ID threshold curves correspond to 15, 20, 30, and 40 mm, respectively. Taking the ID threshold curve corresponding to 15 mm as a reference, the abscissa values of the intersection points of the other 3 ID threshold curves and the reference curve can be obtained as D = 46.7, D = 17.8, and D = 11.8. Before intersecting with the reference curve, the AEP has a positive

**Table 4** Database of AEP, and fitted equations groups

AEP (mm)	Fitted threshold curves corresponding to $\rho_{mix}$ = 2.0 g/cm <sup>3</sup>
15	$I_{2.0} = 16.1 D^{-0.50} D \in [1, 229] (R^2 = 0.99)$
20	$I_{2.0} = 18.2 D^{-0.53} D \in [1, 196] (R^2 = 0.99)$
30	$I_{2.0} = 20.2 D^{-0.58} D \in [1, 136] (R^2 = 0.99)$
40	$I_{2.0} = 23.0 \mathrm{D}^{-0.64} \mathrm{D} \in [1, 96] \ (R^2 = 0.99)$
50	$I_{2.0} = 21.8 \mathrm{D}^{-0.70} \mathrm{D} \in [1, 58] \ (R^2 = 0.99)$
60	$I_{2.0} = 19.3 D^{-0.79} D \in [1, 33] (R^2 = 0.99)$
70	$I_{2.0} = 15.9 D^{-0.91} D \in [1, 19] (R^2 = 0.99)$
80	$I_{2.0} = 12.5 \mathrm{D}^{-0.93} \mathrm{D} \in [1, 19] (R^2 = 0.99)$
90	$I_{2.0} = 10.4 D^{-0.99} D \in [1, 9] (R^2 = 0.99)$
100	$I_{2.0} = 10.4 D^{-0.99} D \in [1, 9] (R^2 = 0.99)$
110	$I_{2.0} = 10.4 D^{-0.99} D \in [1, 9] (R^2 = 0.99)$
120	$I_{2.0} = 10.4 D^{-0.99} D \in [1, 9] (R^2 = 0.99)$

correlation with the triggering rainfall threshold condition, that is, a larger AEP will increase the difficulty of subsequent rainfall triggering debris flow, whereas after intersecting, AEP is inversely related to the triggering rainfall condition.

In Fig. 4b, the six ID threshold curves correspond to 40, 50, 60, 70, 80, and 90 mm, respectively. Because the ID curves corresponding to 100, 110, and 120 mm are same to the curve of 90 mm, they are not drawn within. Taking the ID curve corresponding to 40 mm as the reference, the positions of the other five threshold curves in the I-D coordinate system gradually become lower with the increased AEP, and all of these six curves have no any intersection. This shows that when the AEP exceeds 40 mm in JJG, the AEP and the rainfall threshold condition that triggers debris flow in IJG will have a complete negative correlation. As for the condition of AEP≥90 mm, it can be easily seen from Table 4 that the two key parameters  $\alpha$  and  $\beta$  of the fitting equation tend to be constant. So, the positions of ID curves in the I-D coordinate system cannot change after AEP≥90 mm.

Quantitative analysis of effects of AEP on  $\alpha$  and  $\beta$ 

#### Quantitative analysis of effects of AEP on $\alpha$ and $\beta$

Based on the fitted threshold equations in the form of  $I = \alpha D^{\beta}$ , which can be written logarithmically, as follows:

$$\log I = \log a + \beta \log D \tag{7}$$

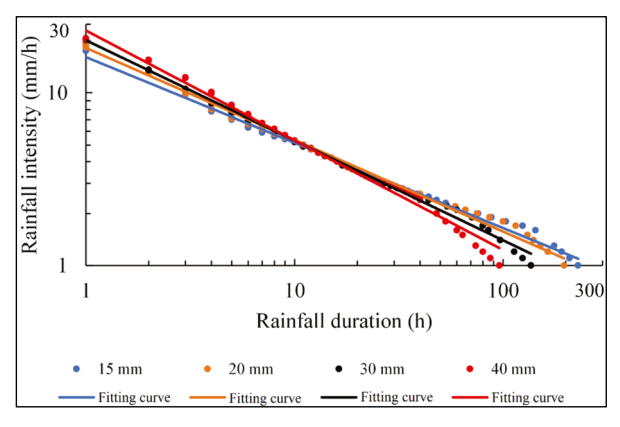
By denoting  $\log I$  as  $Y_D$ ,  $\log D$  as  $X_D$ , and  $\log \alpha$  as  $B_\alpha$ , Eq. 7 can be rewritten as follows:

$$Y_I = \beta X_D + B_a \tag{8}$$

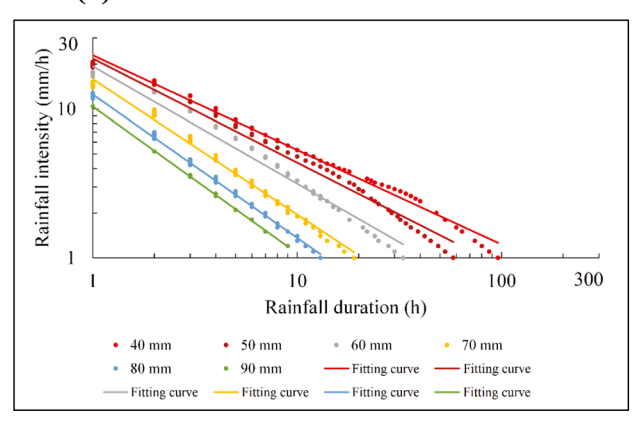
According to Eqs. 7 and 8, when D is equal to 1 h,  $I = \alpha$ .  $\alpha$  is numerically equal to the value of  $I_{D=1}$  in the condition of D=1, and thus, a represents the critical rainfall intensity required to trigger a debris flow for D=1 h. From a geometrical point of view, Eq. 8 is represented by a linear equation in Fig. 4, where log a is the intercept of the linear equation on the vertical axis and  $\beta$  is the slope of the linear line. The absolute value of  $\beta$  represents the deceleration rate of rainfall intensity with increasing rainfall duration, that is, the rate of decrease from  $I_{D=1}$  to 1 mm/h. As shown in Fig. 4, AEP can change the position of the ID threshold curve in the I-D coordinate system and accordingly change the fitted parameters of the ID threshold curve of debris flow, α and β. Therefore, the relationship between these two fitting parameters and AEP can characterize the movement law of the ID threshold curve in the I-D coordinate system caused by AEP change. Based on the data sets of  $\alpha$  and AEP in Table 4, the effect of AEP on a is described by the following equations, which were fitted using the least square method:

$$\begin{cases} \alpha = -0.006AEP^{2} + 0.5AEP + 10.6 & 15 \le AEP < 90\\ \alpha = 10.4 & 90 \le AEP \le 120 \end{cases}$$
 (9)

In the condition of 15 mm  $\leq$  AEP  $\leq$  90 mm,  $\alpha$  represents parabolic variation with AEP. Interestingly, a does not always decrease with continuously increasing AEP. When AEP  $\leq$  40 mm, the  $\alpha$  values necessary for triggering a debris flow increase simultaneously with AEP; when AEP > 40 mm, α decreases with increasing AEP, but the decrease does not continue indefinitely with increasing AEP, because for AEP > 90 mm,  $\alpha$  is constant at 10.4.



(a) Fitting curves in the conditions of 15 mm≤ AEP≤40 mm



**(b)** Fitting curves in the conditions of 40 mm≤ AEP≤90 mm

Fig. 4 ID curves corresponding to different AEP

The AEP in the parabolic segment varies from 15 to 90 mm, and the parabola described by Eq. 9 is plotted in Fig. 5. Since  $\alpha$  is numerically equal to  $I_{D=1}$ , the AEP- $\alpha$  relationship in Fig. 5 can reflect the variation law of the longitudinal intercept of each ID threshold curve with AEP. When 15 mm ≤ AEP ≤ 40 mm, the longitudinal intercept of each threshold curve in Fig. 4a increases parabolically. Before the ID threshold curves intersect in Fig. 4a, the increasing longitudinal intercept is the superficial reason that the ID threshold conditions necessary for triggering debris flow in JJG show a positive correlation with the AEP. When 40 mm≤AEP≤90 mm, the longitudinal intercept of each threshold curve in Fig. 4b decreases parabolically, and the relationship between the ID threshold condition and AEP begins to show a negative correlation. B represents the slope of the ID threshold curve in Fig. 4 and is less than o. The main reason of  $\beta$  < 0 is a tradeoff between rainfall intensity and rainfall duration in order to trigger debris flow in nature. Based on the data sets of  $\beta$  and AEP in Table 4, the effect of AEP on  $\beta$  is described by the following Eqs. (10), which were fitted using the least square method. As shown by Eq. 10, as AEP increases from 15 to 90 mm, β decreases linearly. When AEP exceeds 90 mm,  $\beta$  becomes a constant with a value of -0.99.

$$\begin{cases} \beta = -0.007AEP - 0.4 & 15 \le AEP \le 90\\ \beta = -0.99 & 90 \le AEP \le 120 \end{cases}$$
 (10)

The line segment with the AEP varying between 15 and 90 mm was plotted in Fig. 6. In the condition of 15 mm  $\leq$  AEP  $\leq$  90 mm,  $\beta$  and AEP are always negatively correlated without no positive correlation stage like the relationship between  $\alpha$  and AEP, so it can be inferred that  $\beta$  always tends to push the relationship of the AEP and triggering rainfall condition towards negative.

Validation of AEP  $\sim \alpha$  and AEP  $\sim \beta$ .

Based on the historical rainfall data in Table 3, three ID threshold curves for different AEP were fitted using the least square method and listed in Table 5. It should be noted that the amount of field observation data is not sufficient; only three ID threshold curves corresponding to AEP = 20, 30, and 40 mm were obtained. Therefore, only the ID threshold curves corresponding to the three AEP values in Fig. 4a can be calibrated. The three threshold curves derived from Dens-ID are also listed in Table 5.

The six ID threshold curves in Table 5 are plotted in Fig. 7, the axes in which are given on a logarithmic scale. The dashed lines are the ID threshold curve fitted through the observed data, while the solid lines represent the ID threshold curves obtained by Dens-ID. As shown in Fig. 7, the longitudinal intercepts of the three dashed lines increase with AEP. Taking the orange dashed line (the ID curve corresponding to AEP = 20 mm) as a reference, before the other two threshold curves intersect with it, there is a positive correlation between AEP and the triggering rainfall condition, while after intersection with the orange dashed line, AEP and rainfall threshold conditions transformed into a negative correlation. The relationship between AEP and triggering rainfall conditions in Fig. 4a, which was derived by Dens-ID, is consistent with the field observation data.

However, there is a large difference in the  $\alpha$  of the threshold curves fitted by the two methods. The α calculated by Dens-ID is commonly larger than that derived from observation data. Taking the black lines (including black solid and dashed lines) corresponding to AEP = 30 mm as instance, the deviation of longitudinal intercept of them is about 7.0 making the position of solid lines higher than that of the dashed lines. Because  $\alpha$  is numerically equal to  $I_{D=1}$ , if taking dashed line with different colors as references, Dens-ID overestimates the triggering rainfall intensity. Two main reasons for the deviation of the α calculated by Dens-ID: (1) according to Zhang et al. (2020), Dens-ID is sensitive to input parameters such as rainfall, hydrology parameters, and soil mechanical parameters, and it is most sensitive to soil cohesion. Unavoidable uncertainties in many input parameters for the physical model can significantly affect the calculation results of Dens-ID (Raia et al. 2014; Zhang et al. 2018; Jacobs et al. 2020); (2) field observation condition for rainfall data: local heavy rainfall in JJG is the main trigger for debris flow. The historical rainfall data in Table 3 were obtained at the rainfall station represented by a red strain (Fig. 2), which is approximately 2 km from Mengian Gully. Because of this spatial deviation, the rain gauge may be unable to detect the center of rainstorms, and thus, the measured rainfall data may be smaller than the actual values. The above two reasons will cause systematic errors in the two methods of deriving ID threshold curves. However, once this systematic error is formed in the model or field observation conditions, the output results will still show a certain evolution law in this limited condition, and the evolution trend from the left boundary to the right boundary of the curve is determined by  $\beta$ .  $\beta$  plays more important role than that of a in the negative correlation of

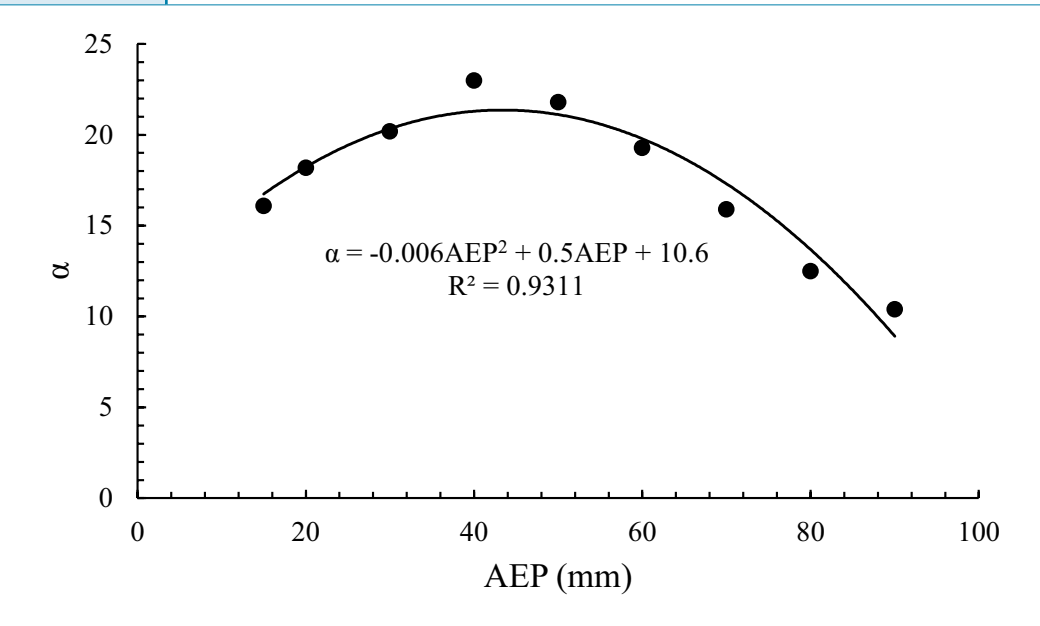
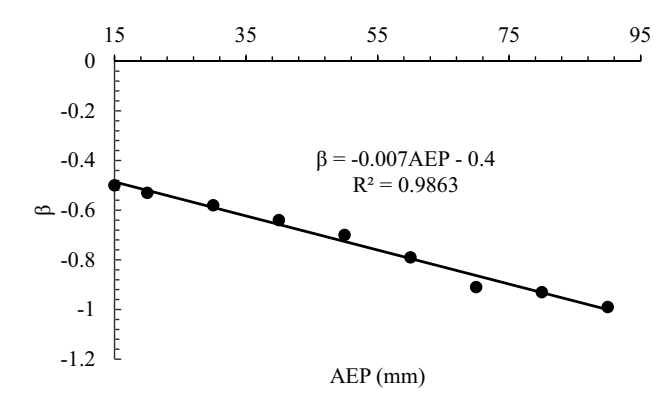


Fig. 5 Function curve describing the relationship between AEP and  $\alpha$ 

AEP and triggering rainfall condition. Only when the β calculated by Dens-ID is close to the value derived from the field observation data can it prove its reliability in describing the hydrological process of the evolution law of rainfall and duration. Fortunately, the  $\beta$  derived from Dens-ID has a smaller error than the  $\alpha$ . Taking the black lines corresponding to AEP = 30 mm as instance, their deviation is about 0.02 making the two black lines nearly parallel. So, the smaller deviation from the observation rainfall data proves that Dens-ID has high credibility in describing the hydrological process that induces the debris flow in JJG.

## Discussions

The larger the AEP, the lower the triggering rainfall condition for debris flow; this qualitative description has almost become a consensus. However, according to the results derived from Dens-ID and field observation data, a larger AEP can only represent a favorable hydrological environment for runoff generation and solid material supply, but it may put forward higher requirements on



**Fig. 6** Function curve describing the relationship between AEP and  $\beta$ 

the triggering rainfall condition. It is necessary to discuss why the increase of the AEP within the range of 15-40 mm can enhance the rainfall triggering conditions of the debris flow in JJG. This finding is confirmed by results derived from Dens-ID and field observations data. So, what mechanism or factors cause this phenomenon is worthy of serious discussion. Debris flow is a result of the mutual game between runoff and solid materials in the channel (Long et al. 2020); this game process can be viewed as whether the hydrodynamic conditions provided by runoff can initiate the loose deposits in the channel (Berti et al. 2020).

In Fig. 4a, before the intersection of any two ID threshold curves, the physical meaning of the longitudinal intercept of each curve can be expressed as the rainfall intensity that can trigger a debris flow is  $I_{D=1}$  when D=1. The coordinate of the longitudinal intercept  $[D=1, I=I_{D=1}]$  is the typical boundary point of the ID threshold curve, which was used to represent the triggering rainfall condition before the intersection of two ID curves. To facilitate the analysis, the  $V_s$  and  $I_{D=1}$  calculated by Dens-ID were normalized, and they are plotted versus AEP (AEP- $V_s$  and AEP- $I_{D=1}$ ) in Fig. 8.  $V_s$ increases continuously for AEP≤40 mm, and it reaches a maximum at AEP = 50 mm. As  $V_s$  increases with increasing AEP, a larger runoff volume  $(V_w)$  is required to bring the debris flow density  $(\rho_{mix})$  to a fixed value of 2.0 g/cm<sup>3</sup>, which requires stronger hydrodynamic conditions, and thus a higher rainfall intensity  $I_{D=1}$ .

**Table 5** Comparison between the fitted ID equations from different ways

AEP (mm)	ID threshold equations				
	Fitted through observation data	Fitted through Dens-ID			
20	$I = 10.6 D^{-0.44}$	$I_{2.0} = 18.2 \mathrm{D}^{-0.53}$			
30	$I = 13.2 D^{-0.60}$	$I_{2.0} = 20.2 D^{-0.58}$			
40	$I = 15.3 D^{-0.78}$	$I_{2.0} = 23.0 D^{-0.64}$			

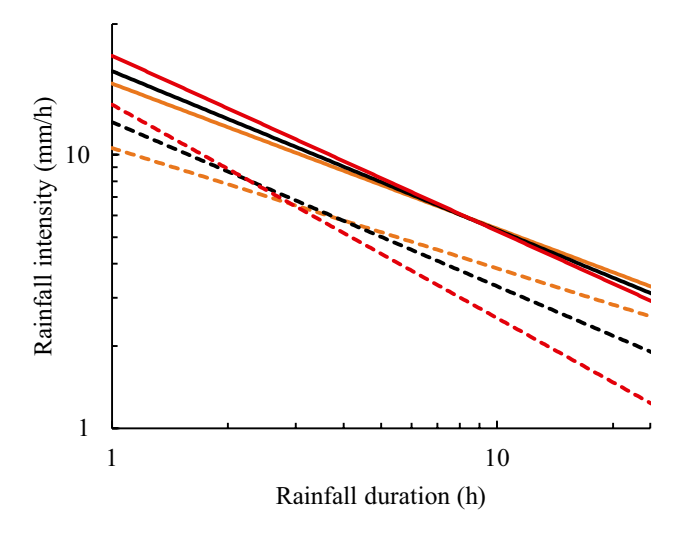


**Fig. 7** ID curves corresponding to different AEP (dashed lines represent curves fitted from the observed rainfall data; solid lines are derived from Dens-ID. Green, red, and black lines represent AEP values of 20, 30, and 40, respectively)

Before point  $P_1$  in Fig. 8, the  $I_{D=1}$  necessary for triggering debris flow in JJG is positively correlated with AEP. Although AEP no longer contributes to the variation of  $V_s$  after AEP reaches 50 mm, the soil-water content can still be increased due to continuously increasing AEP (Zhu and Shao 2008; Schoener and Stone 2020), and accordingly it can enhance the runoff generated rate from rainfall (Castillo et al. 2003; Jones et al. 2017). Under these hydrological conditions, the rainfall intensity  $I_{D=1}$  required to trigger a debris flow with the density of 2.0 g/cm3 decreases gradually; thus, the rainfall condition for triggering debris flow in JJG is negatively correlated with AEP. When AEP exceeds 90 mm ( $P_2$  in Fig. 8),  $I_{D=1}$  stops gradually decreasing and remains constant, indicating that at AEP = 90 mm, the loose solid material in JJG become saturated. Under these hydrological conditions,  $I_{D=1}$  has a constant value of 10.4 mm and does not change with AEP. Therefore, for the two inflection points  $P_1$  and  $P_2$  in Fig. 8, AEP is the external driving factor and operates through the entire process of debris flow formation in JJG.

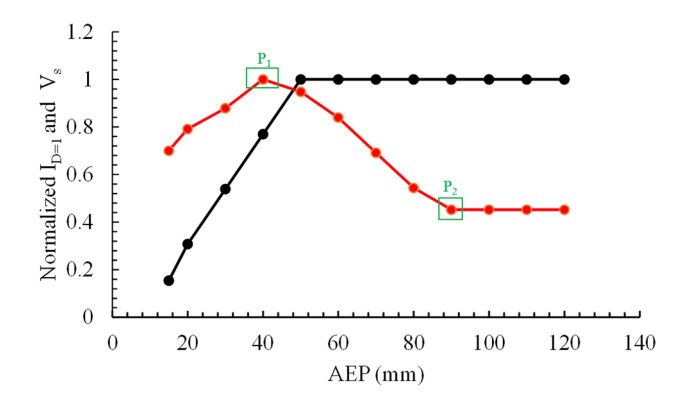


**Fig. 8** AEP- $I_{D=1}$  curve (red line) and AEP- $V_s$  curve (black line)

Tsunetaka et al. (2021) investigated the variation in rainfall patterns for triggering debris flow through field-based, 4-year monitoring in a debris-flow gully. This gully is a part of the Ohya landslide in the southern Japanese Alps indicating supply way of solid material for debris flow is similar to that of JJG. They found that the decrease in sediment storage reduced the rainfall threshold for triggering debris flow. Conversely, after sediment recharge during the subsequent winter, the rainfall condition necessary for debris flow formation is enhanced due to the increase volume of solid material. Although the increase in the volume of solid material may not be caused by AEP, the field findings can show that the increase in solid material supply will instead increase the rainfall conditions triggering debris flow. This finding is basically the same as the calculation results of Dens-ID in JJG.

#### **Conclusions**

Numerical simulation results of Dens-ID show that the rainfall threshold conditions for triggering debris flow in JJG do not always decrease with the increase of AEP. A larger AEP can only represent a favorable hydrological environment for generating runoff and solid materials, but it may put forward higher requirements on the triggering rainfall condition. When AEP > 40 mm, the rainfall threshold condition for triggering debris flow is completely negatively correlated with AEP; however, due to the increase in the solid materials volume in the condition of 15 mm  $\leq$  AEP  $\leq$  40 mm, a stronger hydrodynamic condition is required to trigger the debris flow with a certain density in JJG.

AEP can cause a large difference in the position of the ID threshold curve in the I-D coordinate system indicating that AEP has a significant effect on the triggering rainfall threshold condition. The two derived equations of AEP  $\sim \alpha$  and AEP- $\beta$  can clarify the variation of debris flow ID curves with AEP. The conventional ID threshold curve remains the same regardless of AEP once it is determined. The functions of AEP  $\sim \alpha$  and AEP  $\sim \beta$  can make the originally static ID curve to become a variable threshold in the I-D coordinate system. In this way, the prediction precision of ID curves then can be improved because the effects of AEP on  $\alpha$  and  $\beta$  can be fully considered when they are used to predict debris flow.

## **Funding**

This work was supported by the National Natural Science Foundation of China (No. 42271013, No. 42001100), Chongqing Municipal Bureau of Land, Resources and Housing Administration (KJ-2022033), and Project of the Department of Science and Technology of Sichuan Province (No. 2021YFG0258).

# **Declarations**

**Conflict of interest** The authors declare no competing interests.

#### References

Adams B, Fraser H, Howard C, Hanafy M (1986) Meteorological data analysis for drainage system design. J Environ Eng 112
Baum RL, Savage WZ, Godt JW (2002) TRIGRS-a FORTRAN program for transient rainfall infiltration and grid-based regional slope stability analysis, Virginia, US Geological Survey Open file report, 02–424

- Baum RL, Savage WZ, Godt JW (2008) TRIGRS-a FORTRAN program for transient rainfall infiltration and grid-based regional slope stability analysis, Virginia, US Geological Survey Open file report, 2008-1159
- Bel C, Liébault F, Navratil O, Eckert N, Bellot H, Fontaine F, Laigle D (2017) Rainfall control of debris-flow triggering in the Réal Torrent. Southern French Prealphs, Geomorphology 291:17-32
- Berti M, Bernard M, Gregoretti C, Simoni A (2020) Physical interpretation of rainfall thresholds for runoff-generated debris flows. J Geophys Res Earth Surf 125:e2019JF005513
- Berti M, Simoni A (2005) Experimental evidences and numerical modelling of debris flow initiated by channel runoff. Landslides 3:171–182
- Caine N (1980) The rainfall intensity-duration control of shallow landslides and debris flows. Geogr Ann Ser A Phys Geogr 62:23-27
- Cannon S. Gartner J. Wilson R. Bowers J. Laber J (2008) Storm rainfall conditions for floods and debris flows from recently burned areas in southwestern Colorado and southern California. Geomorphology 96:250-269
- Castillo VM, Gómez-Plaza A, Martínez-Mena M (2003) The role of antecedent soil water content in the runoff response of semiarid catchments: a simulation approach. J Hydrol 284(1-4):114-130
- Chen CY, Chen TC, Yu FC, Yu WH, Tseng CC (2005) Rainfall duration and debris-flow initiated studies for real-time monitoring. Environ Geol 47:715-724
- Chen CW, Oguchi T, Chen H, Lin GW (2018) Estimation of the antecedent rainfall period for mass movements in Taiwan. Environ Ear Sci 77:184
- Chmiel M, Walter F, Wenner M, Zhang Z, Mcardell BW, Hibert C (2020) Machine learning improves debris flow warning. Geophys Res Lett 48:e2020GL090874
- Church M, Jakob M (2020) What is a debris flood? Water Resour Res 56:e2020WR027144
- Coe JA, Kinner DA, Godt JW (2008) Initiation conditions for debris flows generated by runoff at Chalk Cliffs, central Colorado. Geomorpholoav 3:270-297
- Crosta GB, Frattini P (2003) Distributed modeling of shallow landslides triggered by intense rainfall. Nat Hazards Earth Syst Sci 3:81–93
- Cui P, Yang K, Chen J (2003) Relationship between occurrence of debris flow and antecedent precipitation: taking the Jiangjia Gully as an example. China J Soil Water Conserv 1:11-15 (in Chinese)
- Dahal RK, Hasegawa S (2008) Representative rainfall thresholds for landslides in the Nepal Himalaya. Geomorphology 100:429-443
- Gabet EJ, Mudd SM (2006) The mobilization of debris flows from shallow landslides. Geomorphology 1:207-218
- Giannecchini R, Galanti Y, D'Amato AG (2012) Critical rainfall thresholds for triggering shallow landslides in the Serchio River valley (Tuscany, Italy). Nat Hazards Earth Syst Sci 12:829-842
- Glade T, Crozier MJ, Smith P (2000) Applying probability determination to refine landslide-triggering rainfall thresholds using an empirical "Antecedent Daily Rainfall Model." Pure Appl Geophys 157:1059–1079
- Guo XJ, Cui P, Li Y (2013) Debris flow warning threshold based on antecedent rainfall: a case study in Jiangjia Ravine, Yunnan. China J Mount
- Guzzetti F, Peruccacci S, Rossi M, Strak CP (2008) The rainfall intensityduration control of shallow landslides and debris flows: an update. Landslides 5:3-17
- Hasnawir H, Kubota T (2008) Analysis of critical value of rainfall to induce landslides and debris-flow in Mt. Bawakaraeng Caldera, South Sulawesi. Indonesia J Fac Agric Kyushu Univ 53:523–527
- Hirschberg J. Badoux A. McArdell BW. Leonarduzzi E. Molnar P (2021) Evaluating methods for debris-flow prediction based on rainfall in an Alpine catchment. Nat Hazards Earth Syst Sci 21:2773-2789
- Iverson RM, Reid ME, LaHusen RG (1997) Debris flow mobilization from landslides. Annu Rev Earth Planet 25:85–138
- Jacobs L, Kervyn M, Reichenbach P, Rossi M, Marchesini I, Alvioli M, Dewitte O (2020) Regional susceptibility assessments with heterogeneous landslide information: Slope unit- Vs. pixel-based approach. Geomorphology 356:107084
- Jiang ZY, Fan XM, Subramanian SS, Yang F, Tang R, Xu Q, Huang RQ (2021) Probabilistic rainfall thresholds for debris flows occurred after the Wenchuan earthquake using a Bayesian technique. Eng Geo 280:105965

- Jones R, Thomas RE, Peakall J, Manville V (2017) Rainfall-runoff properties of tephra: simulated effects of grain-size and antecedent rainfall. Geomorphology 282:39-51
- Khan YA, Lateh H, Baten MA, Kamil AA (2012) Critical antecedent rainfall conditions for shallow landslides in Chittagong City of Bangladesh. Environ Earth Sci 67:97-106
- Kim SW, Chun KW, Kim M, Catani F, Choi B, Seo J (2021) Effect of antecedent rainfall conditions and their variations on shallow landslidetriggering rainfall thresholds in South Korea. Landslides 18:569–582
- Kim SK, Hong WP, Kim YM (1991) Prediction of rainfall-triggered landslides in Korea. In: Bell DH (ed) Landslides, Proceedings of the 6th International Symposium on Landslides, vol 2. Balkema, Rotterdam, pp 989-994
- Le Bissonnais Y, Renaux B, Delouche H (1995) Interactions between soil properties and moisture content in crust formation, runoff and interrill erosion from tilled loess soils. CATENA 25(1):33-46
- Lehmann P, Or D (2012) Hydromechanical triggering of landslides: from progressive local failures to mass release. Water Resour Res 48:W03535
- Liu DL, Zhang SJ, Yang HJ, Zhao LQ, Jiang YH, Tang D, Leng XP (2016) Application and analysis of debris-flow early warning system in Wenchuan earthquake-affected area. Nat Hazards Earth Syst Sci 16:483-496
- Long K, Zhang SJ, Wei FQ, Hu KH, Zhang Q, Luo Y (2020) A hydrologyprocess based method for correlating debris flow density to rainfall parameters and its application on debris flow prediction. J Hydrol 589:125124
- Luk SH (1985) Effect of antecedent soil moisture content on rainwash erosion. CATENA 12(2-3):129-139
- Marra F, Destro E, Nikolopoulos El, Zoccatelli D, Creutin JD, Guzzetti F, Borga M (2017) Impact of rainfall spatial aggregation on the identification of debris flow occurrence thresholds. Hydrol Earth Syst Sci 21:4525-4532
- Oorthuis R, Hurlimann M, Abanco C, Moya J, Carleo L (2021) Monitoring of rainfall and soil moisture at the Rebaixader catchment (Central Pyrenees). Environ Eng Geosci 27(2):221-229
- Papa MN, Medina V, Ciervo F, Bateman A (2013) Derivation of critical rainfall thresholds for shallow landslides as a tool for debris flow early warning systems. Hydrol Earth Syst Sci 17:4095-4107
- Peres DJ, Cancelliere A (2014) Derivation and evaluation of landslidetriggering thresholds by a Monte Carlo approach. Hydrol Earth Syst Sci 18:4913-4931
- Peres DJ, Cancelliere A (2018) Modeling impacts of climate change on return period of landslide triggering. J Hydrol 567:420-434
- Raia S, Alvioli M, Rossi M, Baum RL, Godt JW, Guzzetti F (2014) Improving predictive power of physically based rainfall-induced shallow landslide models: a probabilistic approach. Geosci Model Dev 7:495-514
- Richards LA (1931) Capillary condition of liquids in porous mediums. Physics 1:318-333
- Ruette JV, Lehmann P, Or D (2014) Effects of rainfall spatial variability and intermittency on shallow landslide triggering patterns at a catchment scale. Water Resour Res 50:7780-7799
- Schoener G, Stone MC (2020) Monitoring soil moisture at the catchment scale – a novel approach combing antecedent precipitation index and radar-derived rainfall data. J Hydrol 589:125155
- Segoni S, Piciullo L, Gariano SL (2018) A review of the recent literature on rainfall thresholds for landslide occurrence. Landslides 15:1483-1501
- Tisdall A (1951) Antecedent soil moisture and its relation to infiltration. Aust J Agric Res 2(3):342-348
- Tsunetaka H, Hotta N, Imaizumi F, Hayakawa YS, Masui T (2021) Variation of rainfall patterns triggering debris flow in the initiation zone of the Ichino-sawa torrent, Ohya landslide. Japan Geomorphol 375:107529
- Yang HJ, Wei FQ, Ma ZF, Gao HY, Su PC, Zhang SJ (2020) Rainfall threshold for landslide activity in Dazhou, southwest China. Landslides 17:61-77
- Yang HJ, Zhang SJ, Hu KH, Wei FQ, Wang K, Liu S (2022) Field observation of debris flow activities in the initiation area of Jiangjia Gully. Yunnan Province, China, Journal of Mountain Science 19(6):1602–16017

- Zhang SJ, Ma ZG, Li YJ, Hu KH, Zhang Q, Li L (2021) A grid-based physical model to analyze the stability of slope unit. Geomorphology 391:107887
- Zhang SJ, Wei FQ, Liu DL, Yang HJ, Jiang YH (2014a) A regional-scale method of forecasting debris flow events based on water-soil coupling mechanism. J Mount Sci 6:1531-1542
- Zhang SJ, Xu CX, Wei FQ, Hu KH, Xu H, Zhao LQ, Zhang GP (2020) A physics-based model to derive rainfall intensity-duration threshold for debris flow. Geomorphology 351:106930
- Zhang SJ, Yang HJ, Wei FQ, Jiang YH, Liu DL (2014b) A model of debris flow forecast based on the water-soil coupling mechanism. J Earth Sci 4:757-763
- Zhang SJ, Zhao LQ, Delgado Tellez R, Bao HJ (2018) A physics-based probabilistic forecasting model for rainfall-induced shallow landslides at regional scale. Nat Hazards Earth Syst Sci 18:969-982
- Zhao BR, Dai Q, Han DW, Dai HC, Mao JQ, Mao JQ, Zhuo L (2019) Probabilistic thresholds for landslides warning by integrating soil moisture conditions with rainfall thresholds. J Hydrol 574:276-287
- Zhu YJ, Shao MG (2008) Variability and pattern of surface moisture on a small-scale hillslope in Liudaogou catchment on the northern Loess Plateau of China. Geoderma 147:185-191

# Shaojie Zhang (☑) • Manyu Xia • Hongjuan Yang • **Fanggiang Wei**

Key Laboratory of Mountain Hazards and Earth Surface Process, Institute of Mountain Hazards and Environment, Chinese Academy of Sciences, Chengdu 610041, China Email: sj-zhang@imde.ac.cn

## Li Li (🖂)

School of Safety Engineering, Chongging University of Science and Technolog, Chongging 401331, China Email: lly\_whu@163.com

### **Dunlong Liu**

College of Software Engineering, Chengdu University of Information and Technology, Chengdu 610225, China

#### Li Li (🖂)

Chongging Natural Resources Safety Dispatch Center, Chongqing 401147, China